A. Alessandrino[1,2]
B. Marelli[2]
C. Arosio[1]
S. Fare[2]
M. C. Tanzi[2]
G. Freddi[1]

[1] Stazione Sperimentale per la Seta, Milano, Italy.

[2] BioMatLab., Bioengineering Dept., Politecnico di Milano, Milano, Italy.

Research Article

Electrospun Silk Fibroin Mats for Tissue Engineering

Processing Silk Fibroin (SF) with electrospinning (ES) offers a very attractive opportunity for producing a variety of 2D and 3D matrices with great potential for tissue regeneration and repair due to the superior biocompatibility and mechanical properties of SF. Different combinations of ES parameters were explored to investigate the best experimental set-up related to the dimension and uniformity of the fibers in the electrospun silk fibroin (ES-SF) mats. Using SEM it was found that the ES-SF mats contain uniform fibers with a diameter in the nanometric range obtained by electrospinning a 7.5 % w/v SF solution in formic acid, with an electric field of 2.4 kV/cm and a spinneret-collector distance of 10 cm. FT-IR and DSC analyses were performed to investigate the structure of the ES-SF mats before and after immersion in methanol for different times (5, 10, and 15 min). The methanol treatment was able to promote the crystallization of SF by conformational transition of random coil and other poorly ordered conformations (turns and bends) to the β-sheet structure. The degree of crystallinity was enhanced as shown by the trend of both the FT-IR crystallinity index and the melting/decomposition peak temperature (from DSC). To study the cytocompatibility of ES-SF mats, tests with L929 murine fibroblasts were carried out. Samples were seeded with the cells and incubated for 1, 3, and 7 days at 37 °C. At each time point, SEM investigations and Alamar blue tests were performed. The SEM images showed cell adhesion and proliferation just after 1 day and cell confluence at 7 days. Alamar blue test demonstrated that there were very low differences between cell viability on ES-SF mats and the tissue culture plastic control.

Keywords: Electrospinning, Cytocompatibility, Silk fibroin

Received: December 13, 2007; *revised:* April 15, 2008; *accepted:* April 17, 2008

DOI: 10.1002/elsc.200700067

1 Introduction

Mimicking the nanometric structures of the extracellular matrix (ECM) is one of the most important goals in tissue engineering. Ideally a scaffold for tissue engineering should mimic the structural and functional profile of the materials found in the native ECM, promoting the formation of a *neo*-tissue without adverse effects in the surrounding tissues [1–7].

Natural fibers in ECM have nanometric or submicrometric dimension and several techniques to produce scaffolds with components in this dimensional range are, nowadays, under investigation [7]. By using the electrospinning (ES) technique it is possible to produce fibrous matrices with nanometric fibers made of several different polymers [8–12]. Using this technique, a polymer solution is pushed, with a controlled flow rate, through a metal needle (spinneret) using a syringe pump. High voltage (usually from 1 kV to 30 kV) is applied and a solid fiber is produced from the drop of a polymer solution present on the tip of the spinneret.

Fiber formation is mainly driven by two effects, the electrostatic repulsion between the charges at the surface of the drop and the coulombic force generated by the electric field between the spinneret and the metallic target (collector) [13]. These electrostatic interactions distort the drop at the nozzle of the spinneret giving to it a conical shape (Taylor cone) and, when the electric field overcomes a threshold value, the two electrostatic contributions win against the surface tension of the polymer solution and a polymer jet starts from the nozzle of the spinneret. Electric forces accelerate the jet by stretching it so that long and thin fibers are formed [8, 13, 14]. The jet has an

Correspondence: A. Alessandrino (antonio.alessandrino@polimi.it), Stazione Sperimentale per la Seta, Via G. Colombo 83, 20133, Milano, Italy.

instability region near the collector where the initially straight polymer jet is whipped or bent and the very thin diameter of fibers is mainly achieved by stretching and acceleration in this region [15].

Silk fibroin (SF) is a natural polymer produced by lepidopters or spiders. The silkworm *Bombyx mori* spins a bave composed of two fibroin filaments coated with sericin, a glue like protein that can be removed with a degumming treatment [16]. Silk fibroin is characterized by a highly repetitive primary sequence that leads to significant homogeneity in the β-sheet secondary structure, high degree of crystallinity and important mechanical properties [17]. These properties, added to the good biocompatibility and the environmental stability of SF provide great opportunity to produce devices for biomedical applications [17–21].

Among the range of techniques useful to process silk fibroin, electrospinning offers a very attractive opportunity for producing a variety of 2D and 3D matrices with great potential for tissue regeneration and repair [8, 17, 22, 23]. Aims of this work were to understand the best electrospinning parameters for processing silk fibroin into mats with uniform morphology and a fiber size as small and homogeneous as possible, to characterize electrospun silk fibroin (ES-SF) mats, and to study their interaction with living cells.

2 Materials and Methods

2.1 Preparation of ES-SF Mats

The silk fibroin aqueous solution was prepared as previously described [20]. Briefly, silk fibroin was degummed in an autoclave at 120 °C for 40 min and than dissolved in a LiBr solution (9.3 M) for 3 h at 60 °C. The solution was then dialyzed for 3 days against distilled water. Silk fibroin films were prepared by pouring 10 mL of the ~1 w % silk fibroin aqueous solution in Petri dishes. Spinning dopes at different polymer concentrations were prepared immediately before spinning by dissolving the films in formic acid.

The electrospinning apparatus is composed of two high voltage generators (F.u.G. Elektronik GmbH – HCN 35-12500) able to generate up to 25 kV. The positive pole is joined to the spinneret, a stainless steel capillary tube with an internal diameter of 0.5 mm, while the negative pole is joined to the collector, an aluminium sheet. A syringe pump (Graseby Medical – MS 2000) pushes the silk fibroin solution from a polypropylene syringe through a PTFE capillary tube up to the spinneret.

Different combinations of electrospinning parameters (see Tab. 1) were explored to investigate the optimal experimental set-up related to the dimension and uniformity of the fibers in the electrospun silk fibroin (ES-SF) mats. In particular, three different solutions were realized solving different concentrations of SF in formic acid (5 %, 7.5 % and 10 % w/v).

The electrospun ES-SF mats were removed from the substrate by treatment with water at 37 °C for 5–10 min followed by isopropanol for 10 min. After an overnight drying at room temperature, the ES-SF mats were immersed in methanol (>99.9 %; CRHOMASOLV® by Sigma-Aldrich) for 5, 10 and 15 min to induce crystallization of silk fibroin [24, 25].

Table 1. Electrospinning parameters.

Concentration [%^w/v]	Solution flow rate [mL/h]	Voltage [kV]	Distance spinneret-collector [cm]
5, 7.5, 10	3, 5, 7	20, 24	7, 10

2.2 Morphological and Chemico-Physical Characterization

For Scanning Electron Microscope (SEM; Joel JSM-6380 LV) observations specimens were mounted onto aluminium stubs, sputter-coated with gold (Bal-Tec Med 020), and observed at different magnification (400–11000×) at an accelerating voltage of 20 kV.

Conformational characterization of ES-SF mats was performed by FT-IR analysis with a Thermo Nicolet 6700 FT-IR Spectrometer equipped with an ATR (Attenuated Total Reflectance) accessory and ZnSe crystal. The crystallinity index was calculated as the intensity ratio between the two amide III components at 1260 cm^{-1} and 1230 cm^{-1} [26].

DSC analysis was performed using a Mettler Toledo DSC-30 in standard aluminium pans. The sample weight was about 1.5–3.5 mg. Samples were heated from 20 °C up to 500 °C under an N_2 atmosphere (scanning rate of 10 °C/min).

2.3 In vitro Cell Interaction

The ES-SF mats were cut by a manual die into small disks (Ø = 6 mm). Before testing, the specimens were quenched with methanol, disinfected in 70 v/v % aqueous ethanol solution for 30 min, dipped into distilled water for 48 h, and washed twice with sterile water. Tissue culture plastic (TCPS, Corning-Costar) was used as negative, non-toxic control for the biological response assessment. The murine fibroblast cell line L929 was obtained from the European Collection of Animal Cell Cultures (ECACC N. 85011425) and cultured at 37 °C with 5 % CO_2 in Dulbecco's Modified Eagle's Medium (DMEM, Sigma-Aldrich) containing 10 % fetal bovine serum (FBS, Sigma-Aldrich) and 1 % penicillin/streptomycin (Sigma-Aldrich). L929 cells were suspended in the culture medium with a density of 7×10^5 cell/mL. The cell suspension (100 µL/well) was seeded onto each ES-SF specimen, placed in a 96-multiwell culture plate and cultured in an incubator (5 % CO_2, 37 °C) up to 7 days. All tests were performed in triplicate. At each time point (1, 3 and 7 days), cell morphology was evaluated by SEM, whereas cell metabolic activity was investigated using the Alamar blue test.

At each time point, the culture medium was replaced with 1 mL Alamar BlueTM (Serotec) solution (10 % v/v in DMEM) and the plate incubated for 4 h. Alamar Blue is a REDOX indicator, i.e. it responds to the reduction or oxidation of the surrounding medium. In this assay it both fluoresces and changes colour in response to the chemical re-

duction of culture medium that results from cell growth and division. 100 μL (3 replicates for each sample) of the medium were removed from each well, were transferred to a 96-well plate and the absorbance was measured using a Tecan Genius Plus plate reader (test wavelength: 570 nm; reference wavelength: 630 nm). The samples were subsequently rinsed with PBS and 1 mL of culture medium was added to each well. The plate was then returned to the incubator for further incubation.

The SF-ES samples seeded with L929 cells were observed by SEM. At each selected time point, specimens were fixed with 1.5 % v/v glutaraldehyde solution, buffered in 0.1 M sodium cacodylate (pH 7.2), dehydrated through a series of ethanol solutions (from 20 % up to 100 % v/v ethanol in distilled water) and air dried. The specimens were sputter-coated as described before and examined by SEM at an accelerating voltage of 10 kV.

3 Results and Discussion

3.1 Morphological and Chemico-Physical Characterization

The morphology of ES-SF mats obtained under different conditions of polymer concentration, voltage, flow rate, and spinneret-collector distance was characterized by SEM, at different magnifications, in order to investigate the effect of electrospinning parameters on the shape and size of SF nanofibers. Typical SEM images of ES-SF mats electrospun with different set-up parameters are shown in Fig. 1. According to the literature [11, 27], at a low polymer concentration ($C_p \leq 5$ w %) the instability of the drop at the tip of the spinneret led to dripping of the polymer solution onto the collector. The drops falling onto the target melted the silk mat leaving holes and/or forming clusters of fused silk nanofibers (see Fig. 1a). An average fiber diameter of 484 ± 114 nm was measured in the regions of the mats where no defects were present (see Fig. 1b).

The formation of beads was another typical feature of sample electrospun at low polymer concentration (Fig. 1c). With increasing polymer concentration up to 7.5 w % and 10 w %, the number of beds decreased or completely disappeared (see Fig. 1d–f). Hence, a $C_p \geq 7.5$ w % was necessary to produce bead-free silk fibers with a submicrometer diameter, at least under the experimental conditions of this study. Electrospinning of SF with $C_p > 10$ w % was attempted but, due to the extremely high viscosity of the solution, it hardly flowed through the capillary and then tended to form a gelled drop at the tip of the spinneret within a few min, thus preventing the onset of nanofibers formation. Other authors succeeded in electrospinning SF at $C_p > 10$ w % [29, 30] but the diverse pre-processing conditions to which SF was subjected before preparation of the electrospinning dope made it difficult to compare the solution properties and the electrospinning results of this study with those previously reported [28].

By investigating the influence of the electric field density (V/cm), non-uniform ribbon-shape fibers were obtained both at the lowest (2 kV/cm) and the highest (~3,4 kV/cm) values of the voltage/distance ratio (see Figs. 1d–e). With respect to the spinneret-collector distance, it was also verified that a

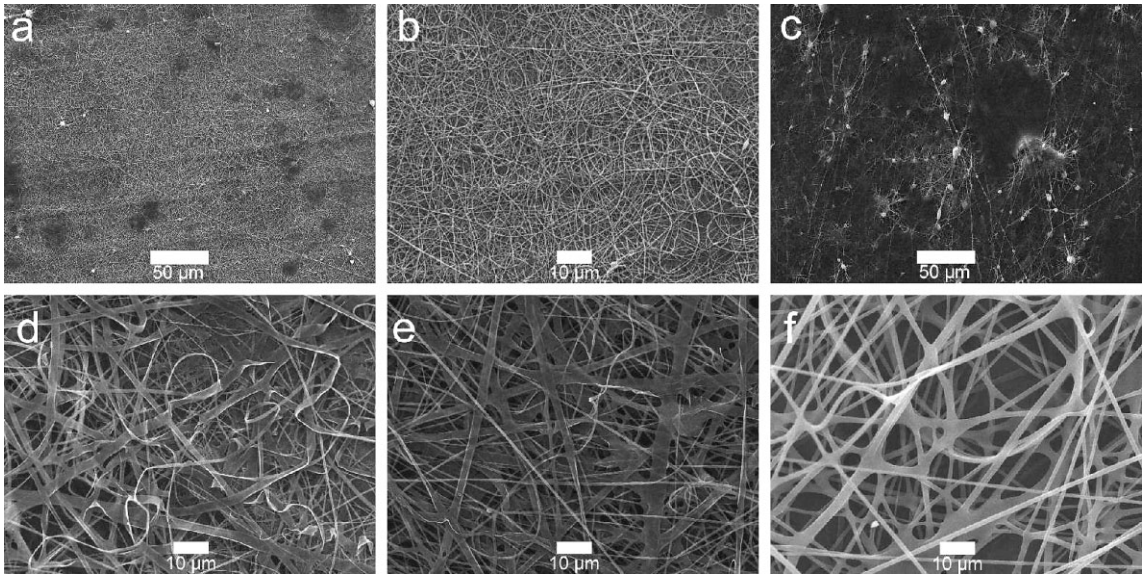

Figure 1. SEM images of ES-SF mats produced using different parameters set-up:
(a) $C_p = 5$ w %, $V = 20$ kV, $f_r = 3$ mL/h, $d = 10$ cm (400×);
(b) $C_p = 5$ w %, $V = 20$ kV, $f_r = 3$ mL/h, $d = 10$ cm (1200×);
(c) $C_p = 5$ w %, $V = 24$ kV, $f_r = 5$ mL/h, $d = 7$ cm (400×);
(d) $C_p = 7.5$ w %, $V = 20$ kV, $f_r = 3$ mL/h, $d = 10$ cm (1200×);
(e) $C_p = 7.5$ w %, $V = 24$ kV, $f_r = 3$ mL/h, $d = 7$ cm (1200×);
(f) $C_p = 10$ w %, $V = 24$ kV, $f_r = 3$ mL/h, $d = 7$ cm (1200×).

minimum distance of 10 cm was necessary to leave enough time for the solvent to completely evaporate and to avoid melting of still wet SF fibers at crossovers. When flow rate values higher than 3 mL/h were used, solvent drops quickly grew at the tip of the spinneret and fell on the mat leading to fused/pierced areas. It was therefore necessary to keep the flow rate at 3 mL/h or below to obtain defect-free ES-SF mats.

The best results in terms of electrospinning performance and properties of ES-SF mats were obtained by using the following set-up of electrospinning parameters: $C_p = 7{,}5$ w %, electric field = 24 kV, spinneret-collector distance = 10 cm, flow rate = 3 mL/h. As shown in Fig. 2, the ES-SF mat was formed by fibers with a more regular and cylindrical shape and with a very smooth surface. The average fiber diameter was 628 ± 107 nm, higher than that obtained at C_p of 5 w %, but still in the nanometer range, with a slightly lower variability in the size of fibers.

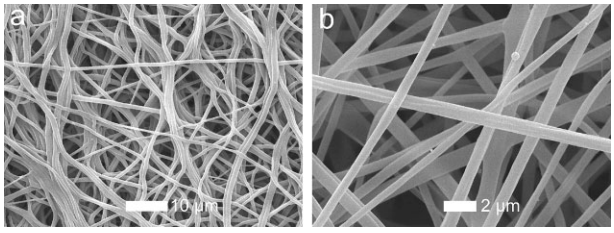

Figure 2. SEM images at different magnification of ES-SF mats produced using $C_p = 7.5$ %, electric field = 24 kV, flow rate = 3 mL/h, spinneret-collector distance = 10 cm.

The secondary structure of regenerated silk fibroin materials could be β-sheet (Silk II), three fold helix (also known as β-turn type II, or Silk I) or random coil [24, 31]. Depending on processing conditions, one conformation could prevail over the others. As it is well known, prevalently amorphous SF materials like cast SF films can be converted into more stable crystalline ones by physical or chemical treatments that are able to promote the crystallization by random coil → β-sheet conformational transition. One of the most common methods used to change the secondary structure is the treatment with organic solvents like alcohols. Dipping a regenerated SF material into methanol is highly effective in inducing the crystallization to the β-sheet structure [23, 24, 32]. Exposition to alcohol vapors is effective as well.

FT-IR spectroscopy is a useful tool to investigate the structural properties and conformational changes of SF materials. The characteristic conformationally sensitive absorption bands of SF are found in the regions of amide I, II, and III falling at about 1625 cm^{-1}, 1528 cm^{-1}, and 1230 cm^{-1}, respectively [24, 31, 32]. In this study, the attention was focused on the spectral changes of the Amide I peak as a function of the time of immersion into methanol (see Fig. 3). The use of peak deconvolution tools (*Peak Fitting Module, Origin v. 7.0*) allowed the most important spectral components falling in this crowded wavenumbers range to be identified. Before the methanol treatment, the ES-SF mat showed a main absorption at 1621 cm^{-1} attributed to the β-sheet conformation, and a

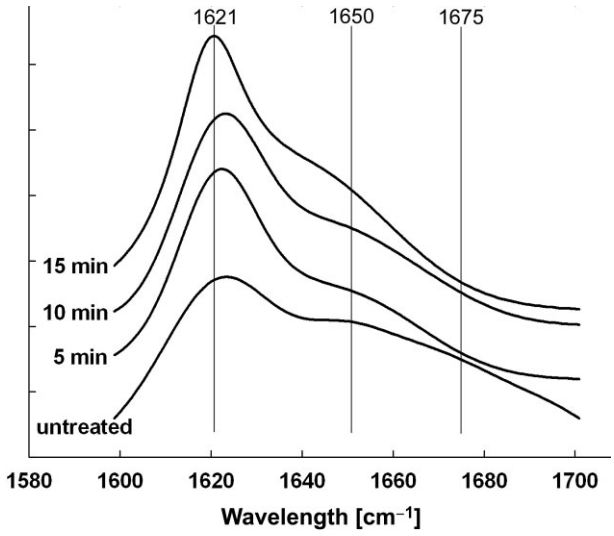

Figure 3. Amide I region of the FT-IR spectra of ES-SF mats before (untreated) and after the treatment with methanol for different times.

range of medium-to-small intensity absorptions at higher wavenumbers (~1640–1700 cm^{-1}) attributed to random coil and to various types of turns and bends [24]. The presence of an intense β-sheet band in the IR spectrum of SF nanofibers electrospun from a formic acid solution can be related to the combined effect of the solvent, which is known to promote the formation of β-sheet crystallites on drying [28], and of the washing procedure (water + isopropanol) used to remove the electrospun ES-SF mat from the substrate.

The relative intensity of the β-sheet peak at 1621 cm^{-1} increased by immersion in methanol while that of the other amide I contributions at higher wavenumbers decreased. Interestingly, the effect was evident even at the shortest dipping time of 5 min. Therefore, the methanol treatment promoted the transition of amorphous and less ordered secondary structures into the more ordered β-sheet structures, thus reducing the intrinsic structural heterogeneity of SF nanofibers. The contribution of methanol to achieve a more refined structure was also confirmed by the behavior of the IR crystallinity index, which increased gradually as a function of the immersion time (see Fig. 4).

DSC analyses evidenced differences in the thermal behavior of the ES-SF samples before and after methanol treatment for 5, 10 and 15 min (see Fig. 5). The sample before methanol treatment showed two weak and broad endothermic transitions at about 180 °C and 215 °C, followed by a more intense endotherm peaking at 280 °C. While the latter is attributed to melting/decomposition of SF chains with non-oriented and poorly crystalline structure, the transitions falling at lower temperature can be related to thermal motions and/or melting phenomena involving amorphous SF chain segments. Although β-sheet crystallites were already present in the SF nanofibers even before methanol treatment, their level of organization was still quite poor, just enough to ensure the formation of short-range ordered SF domains immersed in a disordered matrix with lower thermal stability [24].

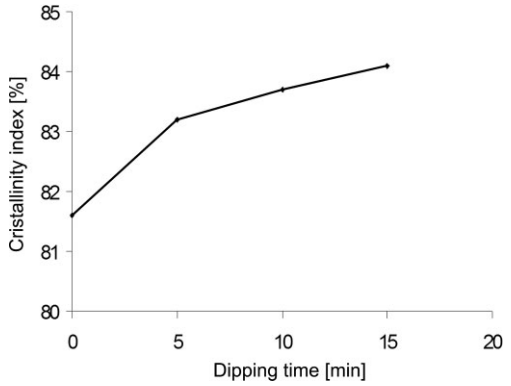

Figure 4. Trend of the crystallinity index calculated as a ratio between the amide III absorption bands at 1265 cm^{-1} and 1235 cm^{-1} as a function of the dipping time in methanol.

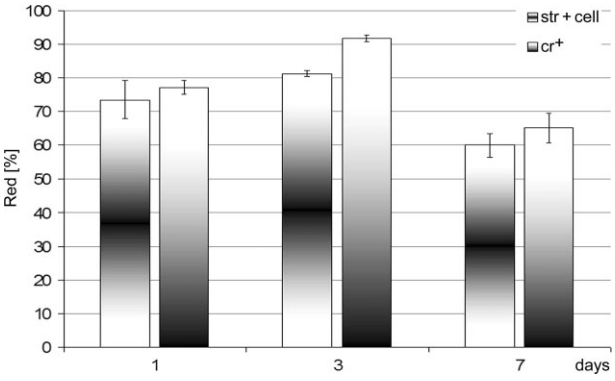

Figure 5. DSC thermograms of ES-SF before (untreated) and after the treatment with methanol for different times.

ES-SF mats after methanol treatment did not show any evidence of the presence of low temperature endothermic peaks between 160 °C and 220 °C. In accordance with FT-IR analyses, after dipping ES-SF mats in methanol some amorphous structures were turned into crystalline ones. Methanol was probably able to induce the formation of long-range ordered structures which restricted the thermally induced molecular motion of SF chains and, therefore, no thermal transitions were noticed in this temperature range already after a 5 min treatment.

With reference to the melting/decomposition transition falling at 280 °C, the treatment with methanol caused a significant sharpening of the peak and a shift to higher temperature until about 288 °C. This trend is closely similar to that reported for amorphous regenerated SF materials, such as films, subjected to treatments able to induce the β-sheet crystallization of SF [33]. With increasing the dipping time from 5 to 15 min, a shoulder of the main melting/decomposition peak appeared in the high temperature range at above 300 °C. Since this transition has been observed in other SF materials regenerated from formic acid and has been attributed to thermal degradation of oriented β-sheet regions [24], the presence of this new peak in the ES-SF mats, as well as the sharpening and high temperature shift of the main peak in this region, point out that the methanol treatment was effective in developing SF nanofibers with a more regular and better organized crystalline texture by transforming part of the amorphous regions into more crystalline domains.

3.2 In vitro L929 Cell Interaction

The evaluation of the absorbance value, related to the percentage of Alamar Blue reduction, allows to obtain information about cell vitality onto the ES-SF mats (str+cell) in comparison to that in the TCPS well (cr^+). One day after L929 seeding, it is possible to observe an absorbance value similar to that of the control (see Fig. 6), and after 3 days, an increase in cell proliferation (i.e. higher absorbance value), meaning that the ES-SF structure appeared adequate for cell colonization. After 7 days from seeding, cells came to an almost complete confluence, so that the absorbance values showed a decrease due to cell suffering onto both the ES-SF and control structures (see Fig. 6).

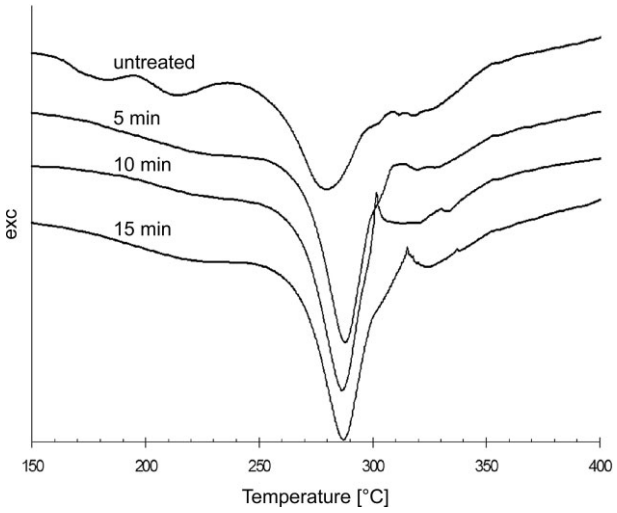

Figure 6. Cell proliferation assessed by Alamar Blue test (1, 2, 7 days) of L929 cell culturing onto ES-SF (str+cell) and TCPS (cr^+).

SEM observation confirmed the results of the biochemical assay. In particular, after 1 day from the seeding it is possible to observe that cells appeared well adhered onto the ES-SF structure (see Fig. 7a); after 3 days, L929 cells have completely colonized the substrate, showing a good integration with the SF matrix (see Fig. 7b). SF nanofibers were completely covered by cells that have proliferated also under the surface of the structure, demonstrating that mat porosity was adequate for cell colonization. Moreover, after 7 days, cells have covered all the specimen (see Fig. 7c). Interestingly, they did not only adhere and proliferate on the structure but also penetrate into the scaffold (see Fig. 7d).

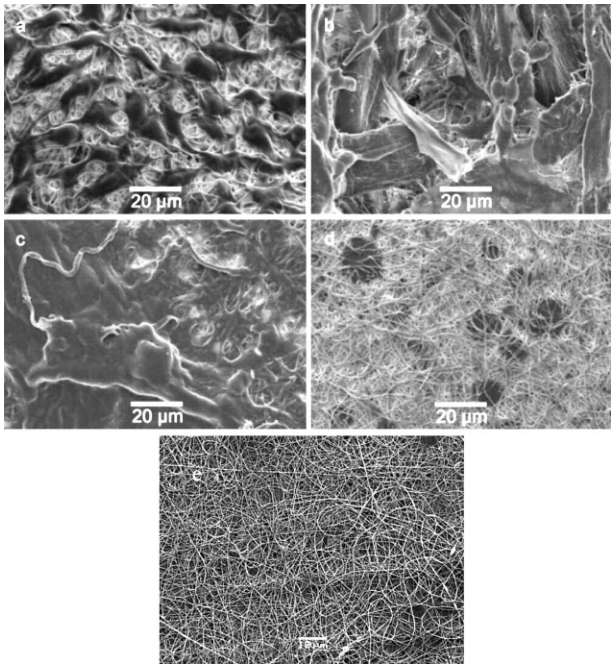

Figure 7. SEM micrographs of L929 cells seeded onto the ES-SF structure after (a) 1 day, (b) 3 days, (c) 7 days, (d) 7 days (side in contact with the bottom of the well). (e) SEM micrographs of the control ES-SF structure.

4 Conclusions

In this study, working parameters suitable to electrospin silk fibroin mats were investigated and the ES-SF mats thus produced were characterized. SEM observations showed that more uniform mats with regular morphology and fibers in the nanometric range were obtained by using a polymer concentration of 7.5 w%, a voltage of 24 kV, a flow rate of 3 mL/h, and a spinneret-collector distance of 10 cm. Lower polymer concentration, shorter spinneret-collector distance, and higher flow rate led to various kinds of defects, such as non continuous fibers, beads, dripping of drops onto the neo-formed mat, fusing of wet fibers, etc., thus leading to poor quality ES-SF mats. Ribbon-like fibers were also produced at low and high values of the voltage/distance ratio, indicating that this is a key parameter for the production of SF nanofibers with uniform size and cylindrical shape.

FTIR and DSC analyses showed that the structure of the *neo*-formed ES-SF mats was improved at the molecular level by a methanol treatment which was effective in increasing the degree of crystallinity and the thermal stability of SF nanofibers by inducing the conformational transition of amorphous domains into more crystalline ones.

Nanometric electrospun SF fibers, with a size similar to that of the natural ECM fibers, were able to promote adhesion, spreading and proliferation of L929 cells. Just after day 1, cells showed good adhesion and after day 7, layered cells were observed and cells confluence was almost achieved. After 7 days in cell culture, some cells were noticed on the bottom side of the samples. This finding is in accordance with that recently reported by Zhang et al., and points out that the porosity of the electrospun SF mats allows cells to penetrate and colonize the whole matrix [34].

In conclusion, the results reported in this study demonstrate the suitability of ES-SF mats from both the morphological (fiber size and porosity)/structural (stability), and biological (cytocompatibility) point of view to be used as tissue engineering matrices in tissue regeneration of skin and other bi-dimensional tissues.

References

[1] A. Greiner, J. H. Wendorff, A. L. Yarin, E. Zussman, Biohybrid nanosystems with polymer nanofibers and nanotubes, *Appl. Microbiol. Biotechnol.* **2006**, *71 (4)*, 387–393.

[2] J. A. Matthews, G. E. Wnek, D. G. Simpson, G. L. Bowlin, Electrospinning of collagen nanofibers, *Biomacromolecules* **2002**, *3 (2)*, 232–238.

[3] S. Kidoaki, I. K. Kwon, T. Matsuda, Mesoscopic spatial designs of nano- and microfiber meshes for tissue-engineering matrix and scaffold based on newly devised multilayering and mixing electrospinning techniques, *Biomaterials* **2005**, *26*, 37–46.

[4] C. P. Barnes, S. A. Sell, E. D. Boland, D. G. Simpson, G. L. Bowlin, Nanofiber technology: Designing the next generation of tissue engineering scaffolds, *Adv. Drug Deliv. Rev.* **2007**, *59 (14)*, 1413–1433.

[5] M. Goldberg, R. Langer, X. Jia, Nanostructured materials for applications in drug delivery and tissue engineering, *J. Biomater. Sci. Polym. Ed.* **2007**, *18 (3)*, 241–268.

[6] R. Murugan, S. Ramakrishna, Nano-featured scaffolds for tissue engineering: a review of spinning methodologies, *Tissue Eng.* **2006**, *12 (3)*, 435–447.

[7] Z. M. Huang, Y. Z. Zhang, M. Kotaki, S. Ramakrishna, A review on polymer nanofibers by electrospinning and their applications in nanocomposites, *Composites Sci. Technol.* **2003**, *63 (15)*, 2223–2253.

[8] D. Li, Y. Xia, Electrospinning of nanofibers: Reinventing the wheel? *Adv. Mater.* **2004**, *16 (14)*, 1151–1170.

[9] J. A. Matthews, E. D. Boland, G. E. Wnek, D. G. Simpson, G. L. Bowlin, Electrospinning of collagen type II: a feasibility study, *J. Bioact. Compat. Polym.* **2003**, *18 (2)*, 125–134

[10] W. J. Li, C. T. Laurencin, E. J. Caterson, R. S. Tuan, F. K. Ko, Electrospun nanofibrous structure: a novel scaffold for tissue engineering, *J. Biomed. Mater. Res.* **2002**, *60 (4)*, 613–621.

[11] Q. M. Pham, U. Sharma, A. G. Mikos, Electrospinning of polymeric nanofibers for tissue engineering applications: a review, *Tissue Eng.* **2006**, *12 (5)*, 1197–1211.

[12] C. L. Casper, N. Yamaguchi, K. L. Kiick, J. F. Rabolt, Functionalizing electrospun fibers with biologically relevant macromolecules, *Biomacromolecules* **2005**, *6 (4)*, 1998–2007.

[13] A. Frenot, I. S. Chronakis, Polymer nanofibers assembled by electrospinning, *Curr. Opin. Colloid Interface Sci.* **2003**, *8 (1)*, 64–75.

[14] J. Doshi, D. H. Reneker, Electrospinning process and applications of electrospun fibers, *J. Electrostatics* **1995**, *35 (2–3)*, 151–160.

[15] C. Lu, P. Chen, J. Li, Y. Zhang, Computer simulation of electrospinning, Part I: Effect of solvent in electrospinning, *Polymer* **2006**, *47*, 915–921.

[16] G. Freddi, R. Mosotti, R. Innocenti, Degumming of silk fabric with several proteases, *J. Biotechnol.* **2003**, *106*, 101–112.

[17] C. Veparia, D. L. Kaplan, Silk as a biomaterial, *Prog. Polym. Sci.* **2007**, *32*, 991–1007.

[18] G. H. Altman, F. Diaz, C. Jakuba, T. Calabro, R. L. Horan, J. Chen et al., Silk-based biomaterials, *Biomaterials* **2003**, *24 (3)*, 401–416.

[19] Y. Wang, H. J. Kim, G. Vunjak-Novakovic, D. L. Kaplan, Stem cell-based tissue engineering with silk biomaterials, *Biomaterials* **2006**, *27 (36)*, 6064–6082.

[20] T. Arai, G. Freddi, R. Innocenti, M. Tsukada, Biodegradation of *Bombyx mori* silk fibroin fibers and films, *J. Appl. Polym. Sci.* **2004**, *91*, 2383–2390.

[21] R. L. Horan, K. Antle, A. L. Collette, Y. Wang, J. Huang, J. E. Moreau et al., In vitro degradation of silk fibroin, *Biomaterials* **2005**, *26 (17)*, 3385–3393.

[22] S. Sukigara, M. Gandhi, J. Ayutsede, M. Micklus, F. Ko, Regeneration of *Bombyx mori* silk by electrospinning, Part 1: processing parameters and geometric properties, *Polymer* **2003**, *44 (19)*, 5721–5727.

[23] J. Ayutsede, M. Gandhi, S. Sukigara, M. Micklus, H. E. Chen, F. Ko, Regeneration of *Bombyx mori* silk by electrospinning, Part 3: Characterization of electrospun nonwoven mat, *Polymer* **2005**, *46 (5)*, 1625–1634.

[24] D. Wilson, R. Valluzzi, D. Kaplan, Conformational transitions in model silk peptides, *Biophys. J.* **2000**, *78 (5)*, 2690–2701.

[25] M. Tsukada, Y. Gotoh, M. Nagura, N. Minoura, N. Kasai, G. Freddi, Structural changes of silk fibroin membranes induced by immersion in methanol aqueous solutions, *J. Polymer Sci. Part B: Polymer Physics* **1994**, *32 (5)*, 961–968.

[26] G. Freddi, G. Pessina, M. Tsukada, Swelling and dissolution of silk fibroin (*Bombyx mori*) in N-methyl morpholine N-oxide, *Int. J. Biol. Macromol.* **1999**, *24 (2–3)*, 251–263.

[27] J. M. Deitzel, J. Kleinmeyer, D. Harris, N. C. B. Tan, The effect of processing variables on the morphology of electrospun nanofibers and textiles, *Polymer* **2001**, *42*, 261–272.

[28] I. C. Um, H. Y. Kweon, Y. H. Park, S. Hudson, Structural characteristics and properties of the regenerated silk fibroin prepared from formic acid, *Int. J. Biol. Macromol.* **2001**, *29 (2)*, 91–97.

[29] B. M. Min, G. Lee, S. H. Kim, Y. S. Nam, T. S. Leb, W. H. Park, Electrospinning of silk fibroin nanofibers and its effect on the adhesion and spreading of normal human keratinocytes and fibroblasts in vitro, *Biomaterials* **2004**, *25*, 1289–1297.

[30] K.-H. Kim, L. Jeong, H. N. Park, S. Y. Shin, W. H. Park, S. C. Lee et al., Biological efficacy of silk fibroin nanofiber membranes for guided bone regeneration, *J. Biotechnol.* **2005**, *120*, 327–339.

[31] X. Chen, D. P. Knight, Z. Shao, F. Vollrath, Regenerated *Bombyx mori* silk solutions studied with rheometry and FTIR, *Polymer* **2001**, *42 (25)*, 9969–9974.

[32] B. M. Min, L. Jeong, K. Y. Lee, W. H. Park, Regenerated silk fibroin nanofibers: water vapor-induced structural changes and their effects on the behavior of normal human cells, *Macromol. Biosci.* **2006**, *6 (4)*, 285–292.

[33] J. Magoshi, M. Mizuide, Y. Magoshi, K. Takahashi, M. Kubo, S. Nakamura, Physical properties and structure of silk: VI. Conformational changes in silk fibroin induced by immersion in water at 21–130 °C, *J. Polym. Sci.: Polym. Phys. Ed.* **1979**, *17*, 515–520.

[34] Y. Zhang, C. T. Lim, S. Ramakrishna, Z. M. Huang, Recent development of polymer nanofibers for biomedical and biotechnological applications, *J. Mater. Sci. Mater. Med.* **2005**, *16 (10)*, 933–946.

